

SARD: Segmentation-Aware Anomaly Synthesis via Region-Constrained Diffusion with Discriminative Mask Guidance

Yanshu Wang¹, Xichen Xu¹, Xiaoning Lei², and Guoyang Xie²

¹Global Institute of Future Technology, Shanghai Jiao Tong University, Shanghai, China

²Department of Intelligent Manufacturing, CATL, Ningde, China

isaac_wang@sjtu.edu.cn, neptune_2333@sjtu.edu.cn, leixn01@outlook.com, guoyang.xie@ieee.org

Abstract—Synthesizing realistic and spatially precise anomalies is crucial for improving the robustness of industrial anomaly detection systems. Recent diffusion-based methods have shown promise in modeling complex defect patterns, yet they often lack spatial controllability and fail to preserve fine-grained regional fidelity. To address these limitations, we propose SARD (Segmentation-Aware anomaly synthesis via Region-constrained Diffusion with discriminative mask Guidance), a novel diffusion-based framework tailored for anomaly generation. Specifically, we introduce a *Region-Constrained Diffusion* (RCD) process that freezes the background and selectively updates only the foreground anomaly regions during reverse denoising, effectively suppressing background artifacts. In addition, a *Discriminative Mask Guidance* (DMG) module is incorporated into the discriminator to jointly assess global realism and local anomaly fidelity, guided by pixel-level masks. Extensive experiments on the MVTec-AD and BTAD datasets demonstrate that SARD outperforms existing methods in terms of segmentation accuracy and visual quality, establishing a new state-of-the-art for pixel-level anomaly synthesis.

Index Terms—Industrial anomaly synthesis, Industrial anomaly segmentation

I. INTRODUCTION

Industrial anomaly segmentation is essential for automated visual inspection in modern manufacturing, as it enables fine-grained pixel-level localization of defects. Compared to image-level detection, segmentation offers significantly more actionable insights for high-resolution quality control. However, acquiring large-scale, accurately annotated segmentation masks is notoriously challenging due to the rarity, diversity, and annotation costs associated with real-world anomalies. This limitation has spurred increasing interest in synthetic anomaly generation to augment training data and enhance segmentation performance.

Prior works on anomaly synthesis typically rely on heuristic-based manipulations such as patch replacement or texture blending [1], [2]. While simple and interpretable, these approaches often introduce unrealistic artifacts and fail to preserve structural or semantic consistency. GAN-based methods [3], [4] improve generation fidelity but still suffer from unstable training, poor spatial controllability, and difficulty in aligning synthesized anomalies with specific mask regions—particularly for small, localized defects.

Recently, denoising diffusion models [5]–[7] have demonstrated superior generative performance with stable optimization and high sample quality. However, existing diffusion-based anomaly generation frameworks generally treat the image as a whole, without disentangling foreground anomalies from background content. This often leads to degraded background fidelity, blurry or misaligned anomalies, and limited controllability in synthesized outputs.

To overcome these challenges, we propose **SARD** (Segmentation-Aware Anomaly Synthesis via Region-Constrained Diffusion), a novel diffusion-based framework tailored for pixel-level anomaly synthesis. Our approach introduces two key innovations:

- **Region-Constrained Diffusion (RCD)**: Instead of updating the entire image during reverse diffusion, RCD confines the denoising process to foreground anomaly regions, preserving background consistency by reusing the forward-diffused clean image. This constraint ensures the model focuses its generative capacity on learning defect textures, avoiding unnecessary alteration of normal areas.
- **Discriminative Mask Guidance (DMG)**: We design a dual-branch discriminator that jointly evaluates global realism and region-specific fidelity. The foreground-aware branch leverages binary anomaly masks to compute localized adversarial losses, guiding the generator to produce sharper and mask-aligned anomalies.

We evaluate **SARD** on two benchmark datasets: MVTec-AD [8] and BTAD [9], using SegFormer [10] and BiseNet V2 [11] as real-time segmentation backbones. Extensive comparisons with representative methods—including CutPaste [1], DRAEM [2], GLASS [12], DFMGAN [4], RealNet [13], AnomalyDiffusion [14], and DDGAN [15]—show that SARD significantly improves downstream segmentation performance.

Furthermore, ablation studies confirm the effectiveness of RCD and DMG in enhancing spatial alignment, texture realism, and segmentation-friendliness of the generated anomalies. By explicitly modeling foreground-background separation and introducing region-specific supervision, SARD establishes a new state-of-the-art in diffusion-based anomaly synthesis for

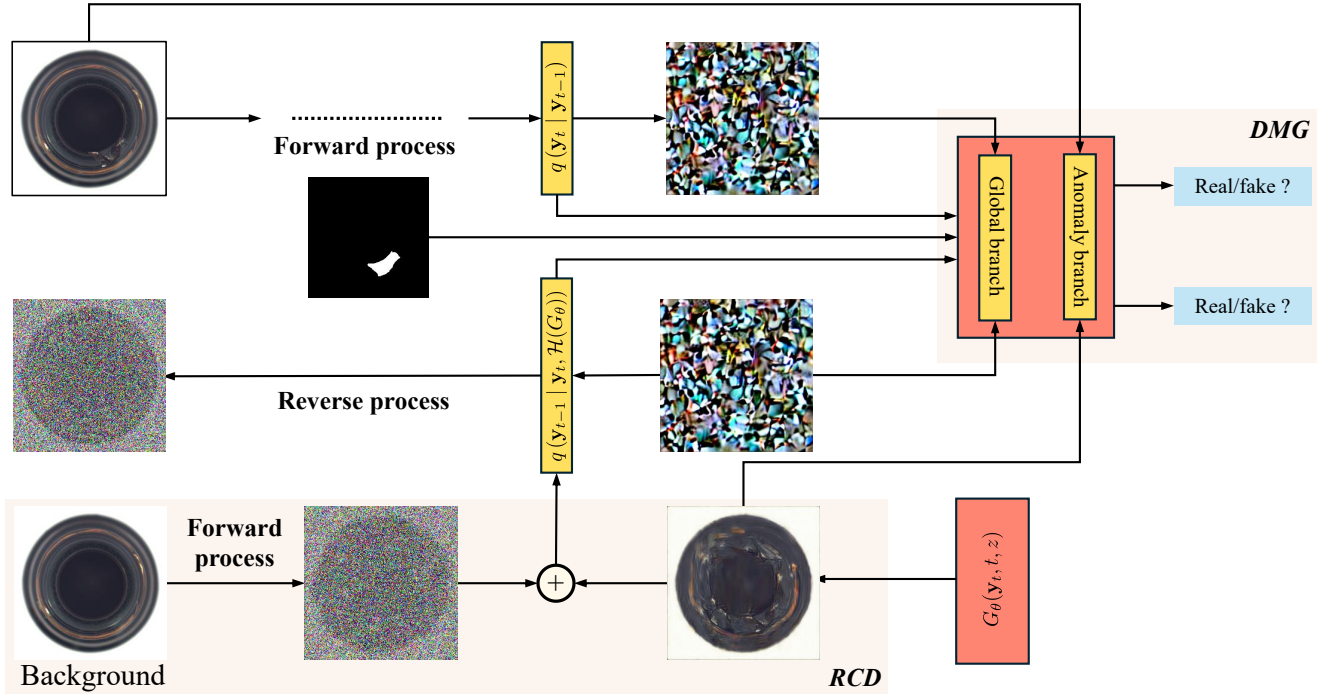


Fig. 1. Overview of the proposed SARD framework. At each reverse diffusion step, the generator predicts a clean image, which is used to sample a posterior estimate. Region-Constrained Diffusion (RCD) fuses this sample with the noisy input, preserving background regions while updating only the anomaly area. A dual-branch discriminator enforces both global realism and mask-guided local fidelity.

industrial visual inspection.

II. RELATED WORK

Anomaly Synthesis. To alleviate the scarcity of annotated industrial anomalies, a variety of strategies have been explored for synthetic anomaly generation in recent years. Early training-free approaches, such as CutPaste and DRAEM [1], [2], rely on heuristic manipulations like patch replacement or image reconstruction to simulate anomaly patterns. However, these methods often produce artifacts, lack semantic alignment, or exhibit limited structural consistency, which may hinder their effectiveness in real-world applications.

GAN-based methods [3], [16], [17], including representative approaches such as DFMGAN [4], aim to enhance generation realism through adversarial training. While these models can produce more plausible textures and sharper boundaries, they still face challenges in terms of spatial controllability, precise localization, and reliable alignment between generated anomalies and designated regions.

Diffusion-based methods [5]–[7] have recently emerged as strong alternatives, offering stable training dynamics and high-fidelity synthesis through iterative refinement. For example, DDGAN [15] introduces adversarial feedback into the reverse diffusion process to accelerate sampling while maintaining quality, whereas AnomalyDiffusion [14] leverages diffusion priors for anomaly representation and modeling. Nonetheless, many of these approaches treat the image as a whole, without explicitly separating foreground anomalies from background content, which can lead to visual incoherence or contextual

inconsistency. Segmentation-aware synthesis techniques such as GLASS [12] and Synth4Seg [18] attempt to mitigate this by incorporating geometric constraints or mask supervision, although the degree of foreground-background decoupling remains limited in practice.

Anomaly Segmentation. Pixel-wise anomaly segmentation plays a critical role in industrial inspection and visual quality control, yet remains difficult due to the rarity, diversity, and subtle appearance of real-world defects. Traditional approaches, including both reconstruction-based and feature-based pipelines [19]–[21], often rely on assumptions of normality but struggle to accurately localize small-scale, sparse, or low-contrast anomalies. These limitations are particularly pronounced in fine-grained defect scenarios.

To overcome these challenges, synthetic data augmentation has emerged as a promising direction. Methods such as GLASS, Synth4Seg, and RealNet utilize synthesized anomalies during training to improve segmentation performance under limited annotation conditions. These works emphasize the importance of structural realism, spatial precision, and mask fidelity in the generation process. Evaluations are typically carried out using lightweight and real-time segmentation backbones, including SegFormer [10] and BiseNet V2 [11], ensuring computational efficiency and consistent comparisons across benchmarks.

III. PROPOSED METHOD

Given normal images and their corresponding anomaly masks, our goal is to generate synthetic anomalies that are

both realistic and precisely aligned with the masks, enabling downstream segmentation models to learn robust detection boundaries. To this end, we introduce a novel diffusion-based framework comprising two key components: (i) **Region-Constrained Diffusion (RCD)** — a modified reverse sampling mechanism that preserves the real background and restricts generation to the foreground anomaly regions; and (ii) **Discriminative Mask Guidance (DMG)** — a discriminator structure that introduces region-specific supervision by focusing on both the entire image and the masked foreground anomaly area. An overview of the framework is illustrated in Fig. 1.

A. Region-Constrained Diffusion (RCD)

In denoising diffusion probabilistic models (DDPM) [5], each reverse step aims to sample a cleaner image \mathbf{x}_{t-1} from a noisy input \mathbf{x}_t . The model defines the posterior distribution over \mathbf{x}_{t-1} as a Gaussian conditioned on the estimated clean image $\hat{\mathbf{x}}_0$:

$$\boldsymbol{\mu}_t = A_t \hat{\mathbf{x}}_0 + B_t \mathbf{x}_t, \quad (1)$$

$$\boldsymbol{\Sigma}_t = \sigma_t^2 \mathbf{I}, \quad (2)$$

$$q(\mathbf{x}_{t-1} | \mathbf{x}_t, \hat{\mathbf{x}}_0) = \mathcal{N}(\boldsymbol{\mu}_t, \boldsymbol{\Sigma}_t), \quad (3)$$

where A_t , B_t , and σ_t^2 are timestep-dependent constants derived from the forward diffusion process. These expressions allow for analytical sampling as long as a reliable prediction of $\hat{\mathbf{x}}_0$ is available.

While DDPM theoretically assumes a Gaussian forward process to enable these closed-form expressions, the assumption becomes less accurate at lower timesteps or in complex data regimes. To flexibly approximate the unknown clean image, we employ a learnable generator G that directly predicts $\hat{\mathbf{x}}_0$ from noisy input:

$$\hat{\mathbf{x}}_0 = G(\mathbf{x}_t, t, \mathbf{z}), \quad (4)$$

where $\mathbf{z} \sim \mathcal{N}(0, \mathbf{I})$ is a latent variable that introduces sample diversity.

However, this standard sampling strategy indiscriminately updates all spatial regions of the image, which is suboptimal for anomaly synthesis. In industrial scenarios, anomalies are typically sparse and localized, and modifying the entire image may degrade background fidelity.

To address this, we introduce **Region-Constrained Diffusion (RCD)**, which incorporates a binary anomaly mask $\mathbf{m} \in \{0, 1\}^{H \times W}$ to restrict updates to anomaly regions. The denoised result is fused with the noisy input as:

$$\mathbf{x}_{t-1} = \mathbf{m} \odot \mathbf{x}'_{t-1} + (1 - \mathbf{m}) \odot \mathbf{x}_t, \quad (6)$$

where \odot denotes element-wise multiplication. This operation preserves the forward trajectory in background regions while allowing targeted refinement of the anomaly areas.

We summarize the masked update as:

$$\mathbf{x}_{t-1} = \mathcal{T}_{\text{rcd}}(\mathbf{x}_t, \hat{\mathbf{x}}_0, \mathbf{m}) := \mathbf{m} \odot \mathbf{x}'_{t-1} + (1 - \mathbf{m}) \odot \mathbf{x}_t. \quad (7)$$

Because the mask is applied post-sampling, the underlying DDPM formulation remains intact. This simple yet effective

mechanism enables spatially controlled generation of anomalies without compromising the realism and consistency of the background.

B. Discriminative Mask Guidance (DMG)

Effective adversarial training relies on the discriminator to provide precise and informative feedback to the generator. In conventional GANs, the discriminator typically operates at the image level, focusing on holistic realism. However, such global supervision often fails to capture subtle, spatially sparse anomalies—particularly in industrial scenarios where defects are small and localized. This motivates the need for a region-sensitive feedback mechanism that can explicitly target foreground anomaly areas.

To this end, we propose **Discriminative Mask Guidance (DMG)**, a dual-branch discriminator structure that jointly evaluates image-level realism and region-specific fidelity guided by anomaly masks.

Let the generated image be $\mathbf{x} \in \mathbb{R}^{C \times H \times W}$, and its associated binary anomaly mask be $\mathbf{m} \in \{0, 1\}^{1 \times H \times W}$. Our discriminator D produces two parallel outputs:

$$D(\mathbf{x}, \mathbf{m}) = (D_{\text{img}}(\mathbf{x}), D_{\text{fg}}(\mathbf{x}, \mathbf{m})), \quad (1)$$

where $D_{\text{img}}(\mathbf{x})$ denotes the global discriminator output assessing holistic realism, while $D_{\text{fg}}(\mathbf{x}, \mathbf{m})$ evaluates the realism of the synthesized anomaly regions using mask-aware supervision.

To compute D_{fg} , we extract intermediate activations $f_l(\mathbf{x}) \in \mathbb{R}^{C' \times H' \times W'}$ from a designated layer l of the discriminator and apply an upsampled binary mask $\text{Up}(\mathbf{m}) \in \{0, 1\}^{1 \times H' \times W'}$. The mask focuses the auxiliary prediction on foreground anomaly regions:

$$D_{\text{fg}}(\mathbf{x}, \mathbf{m}) = \psi(f_l(\mathbf{x}) \odot \text{Up}(\mathbf{m})), \quad (2)$$

where \odot denotes element-wise multiplication, and $\psi(\cdot)$ is a lightweight convolutional head (e.g., one or two layers) applied on masked features. This ensures that discriminator feedback is only activated in regions marked anomalous, promoting targeted supervision.

The overall discriminator loss combines global and foreground components for both real and generated samples:

$$\mathcal{L}_D = \mathbb{E}_{(\mathbf{x}, \mathbf{m}) \sim p_r} [\phi(-D_{\text{img}}(\mathbf{x})) + \lambda \cdot \phi(-D_{\text{fg}}(\mathbf{x}, \mathbf{m}))] + \mathbb{E}_{(\mathbf{x}, \mathbf{m}) \sim p_g} [\phi(D_{\text{img}}(\mathbf{x})) + \lambda \cdot \phi(D_{\text{fg}}(\mathbf{x}, \mathbf{m}))], \quad (3)$$

where $\phi(x) = \log(1 + e^x)$ is the softplus function, and λ is a balancing coefficient (set to 0.2 unless otherwise specified).

During training, both real and synthesized images are paired with binary masks and passed to the dual-branch discriminator. The generator is then optimized to fool both branches by producing samples that are globally realistic and locally consistent with the target anomaly region. This dual perspective effectively enhances anomaly texture quality, boundary precision, and semantic alignment, thereby improving segmentation-aware synthesis performance.

TABLE I
COMPARISON OF PIXEL-LEVEL ANOMALY SEGMENTATION (mIoU/ACC) USING SEGFORMER TRAINED ON SYNTHETIC MVTEC DATA PRODUCED FROM THE PROPOSED SARD AND OTHER EXISTING AS METHODS.

Category	CutPaste		DRAEM		GLASS		RealNet		DFMGAN		AnomalyDiffusion		DDGAN		SARD	
	mIoU ↑	Acc ↑	mIoU ↑	Acc ↑	mIoU ↑	Acc ↑	mIoU ↑	Acc ↑	mIoU ↑	Acc ↑	mIoU ↑	Acc ↑	mIoU ↑	Acc ↑	mIoU ↑	Acc ↑
bottle	75.11	79.49	79.51	84.99	70.26	76.30	77.96	83.90	75.45	80.39	76.39	83.54	66.75	70.70	83.52	87.71
cable	55.40	60.49	64.52	70.77	58.81	62.32	62.51	69.27	62.10	64.87	62.49	74.48	55.83	61.67	70.76	76.60
capsule	35.15	40.29	51.39	62.32	34.12	38.04	46.76	51.91	41.29	15.83	37.73	44.72	40.42	48.74	61.25	71.04
carpet	66.34	77.59	72.57	81.28	70.11	77.56	68.84	79.15	71.33	83.69	64.67	73.59	67.98	79.25	76.39	84.77
grid	29.90	46.72	47.75	67.85	37.43	46.30	37.55	48.86	37.73	54.13	38.70	51.82	47.56	47.99	53.15	67.56
hazel_nut	56.95	60.72	84.22	89.74	55.51	57.43	60.18	63.49	83.43	86.03	59.33	67.48	63.77	68.33	79.30	82.50
leather	57.23	63.49	64.12	71.49	62.05	73.38	68.29	77.16	60.96	68.02	56.45	62.51	58.51	70.41	72.38	80.16
metal_nut	88.78	90.94	93.51	96.10	88.15	90.52	91.28	94.09	92.77	94.93	88.00	91.10	87.27	90.22	94.27	96.55
pill	43.28	47.11	46.99	49.76	41.52	43.54	47.32	58.31	87.19	90.05	83.21	89.00	84.69	90.90	89.02	92.99
screw	25.10	31.35	46.96	59.03	35.94	42.37	47.12	55.17	46.65	50.79	38.47	49.49	37.32	48.07	53.36	64.27
tile	85.33	91.60	89.21	93.74	85.67	90.28	83.53	87.30	88.87	91.96	84.29	89.72	82.42	89.25	90.32	94.77
toothbrush	39.40	63.93	65.35	79.43	53.75	60.46	57.68	72.03	61.00	70.50	48.68	64.41	35.36	40.98	72.77	91.58
transistor	65.03	71.05	59.96	62.18	29.28	30.67	63.71	66.79	73.56	78.48	79.27	91.74	77.96	81.75	89.60	94.24
wood	49.64	60.47	67.52	73.28	50.91	53.16	61.84	89.54	67.00	80.84	60.16	74.62	56.90	62.33	78.85	88.34
zipper	65.39	71.89	69.29	79.36	69.98	79.31	68.78	78.50	66.34	70.50	65.36	72.66	67.09	78.29	72.46	81.65
Average	55.87	63.81	66.86	74.75	56.23	61.44	62.89	71.70	67.71	72.07	62.88	72.06	60.52	67.27	74.53	84.08

The generator is trained using a composite loss that includes global adversarial feedback, foreground-aware adversarial guidance, and a region-weighted reconstruction loss. The full objective is given by:

$$\mathcal{L}_G = \lambda_{\text{img}} \cdot \mathcal{L}_{\text{adv-img}} + \lambda_{\text{mask}} \cdot \mathcal{L}_{\text{adv-mask}} + \alpha \cdot \mathcal{L}_{\text{MSE}}, \quad (4)$$

where:

$$\mathcal{L}_{\text{adv-img}} = \mathbb{E}_{\mathbf{x} \sim p_g} [\phi(-D_{\text{img}}(\mathbf{x}))], \quad (5)$$

$$\mathcal{L}_{\text{adv-mask}} = \mathbb{E}_{\mathbf{x} \sim p_g} [\phi(-D_{\text{fg}}(\mathbf{x}, \mathbf{m}))], \quad (6)$$

and the reconstruction loss is defined as:

$$\mathcal{L}_{\text{MSE}} = \|\mathbf{m} \odot (\hat{\mathbf{x}}_0 - \mathbf{x}_0)\|_2^2 + \beta \cdot \|(1 - \mathbf{m}) \odot (\hat{\mathbf{x}}_0 - \mathbf{x}_0)\|_2^2. \quad (7)$$

Here, $\hat{\mathbf{x}}_0$ is the generator output, \mathbf{x}_0 is the original clean image, and $\mathbf{m} \in \{0, 1\}^{H \times W}$ is the anomaly mask. The softplus activation $\phi(x) = \log(1 + e^x)$ is used for both adversarial terms. The coefficient $\beta < 1$ down-weights the background reconstruction penalty to encourage more accurate anomaly synthesis in foreground regions.

Unless otherwise specified, we use $\lambda_{\text{img}} = 1.0$, $\lambda_{\text{mask}} = 1.0$, $\alpha = 1.0$, and $\beta = 0.1$ in all experiments.

IV. EXPERIMENTS AND RESULTS

A. Implementation Details

Datasets. We conduct experiments on two widely-used industrial anomaly segmentation benchmarks: **MVTec-AD** [8] and **BTAD** [9]. For each anomaly category, we synthesize 500 image-mask pairs using only normal images and randomly generated binary masks. Approximately one-third of the generated samples are used to train the segmentation network, while the remaining two-thirds are held out for evaluation.

Evaluation Metrics. We evaluate segmentation performance using **mean Intersection over Union (mIoU)** and **pixel-wise accuracy (Acc)**, computed between predicted masks and ground-truth anomalies. All metrics are averaged across anomaly categories.

Baselines. We compare our method with six representative anomaly synthesis approaches: CutPaste [1], DRAEM [2], GLASS [12], DFMGAN [4], AnomalyDiffusion [22], and

RealNet [13]. Additionally, we include **DDGAN** [15] as an architectural baseline.

Segmentation Backbones. To assess generalization across architectures, we evaluate all methods using two lightweight real-time segmentation networks: **SegFormer** [10] and **BiseNet V2** [11]. Both models are trained with identical settings on synthetic data generated by each method.

Training Configuration. The generator is trained with 4 discrete diffusion steps using a batch size of 4. We use Adam optimizers with learning rates of 1.6×10^{-4} (generator) and 1.0×10^{-4} (discriminator). An exponential moving average (EMA) with decay rate 0.999 is applied to stabilize generation. The discriminator is updated and regularized via R1 penalty. Training is performed for 20,000 iterations on 2 NVIDIA A800 GPUs.

B. Comparison Studies

Anomaly Segmentation. To evaluate the effectiveness of SARD, we synthesize 500 image-mask pairs for each anomaly type on both MVTec-AD and BTAD using only normal images and binary masks. One-third of these synthetic samples are combined with real labeled pairs for training, and the remaining real samples are used for evaluation. We benchmark SARD against a comprehensive set of anomaly synthesis baselines. All methods are evaluated using SegFormer [10] and BiseNet V2 [11] as segmentation backbones to ensure consistent comparison.

The results on MVTec-AD are reported in Table I. SARD consistently outperforms all baselines in terms of average mIoU and pixel-wise accuracy across the 15 object categories. In particular, on challenging classes such as *capsule*, SARD improves the segmentation mIoU by 9.86% and 14.90% over the second-best methods when using SegFormer and BiseNet V2, respectively. For highly textured or subtle anomaly types like *grid* and *tile*, SARD achieves noticeable gains in structural alignment and background consistency. These results highlight the benefits of our Region-Constrained Diffusion (RCD), which restricts generative updates to foreground regions, and Discriminative Mask Guidance (DMG), which enhances local texture fidelity through region-aware adversarial supervision.

TABLE II
COMPARISON OF PIXEL-LEVEL ANOMALY SEGMENTATION (mIoU/ACC) USING THE REAL-TIME BISENET V2 TRAINED ON SYNTHETIC MVTEC DATA PRODUCED FROM THE PROPOSED SARD AND OTHER EXISTING AS METHODS.

Category	CutPaste		DRAEM		GLASS		RealNet		DFMGAN		AnomalyDiffusion		DDGAN		SARD	
	mIoU ↑	Acc ↑	mIoU ↑	Acc ↑	mIoU ↑	Acc ↑	mIoU ↑	Acc ↑	mIoU ↑	Acc ↑	mIoU ↑	Acc ↑	mIoU ↑	Acc ↑	mIoU ↑	Acc ↑
bottle	71.77	78.57	75.13	79.17	57.81	60.79	72.16	75.55	64.28	71.31	75.28	85.11	61.25	65.97	81.70	90.79
cable	46.00	57.08	53.88	60.96	16.63	16.65	51.22	62.32	57.09	63.25	60.55	74.96	48.03	56.45	70.24	79.06
capsule	25.97	37.04	36.82	42.19	19.53	51.89	35.97	39.39	28.40	31.18	26.77	32.87	33.49	42.64	51.72	64.24
carpet	58.98	72.22	68.42	77.21	64.77	73.93	8.98	9.01	62.13	67.98	58.18	64.69	61.59	73.52	70.13	82.69
grid	24.68	44.17	42.81	63.34	6.50	6.91	10.61	11.47	10.17	15.23	18.98	24.30	2.94	2.83	38.53	55.13
hazel_nut	47.93	53.57	74.83	81.35	71.54	75.62	60.16	65.93	79.78	84.37	57.26	70.41	55.37	62.76	78.34	85.22
leather	31.11	58.36	55.07	61.58	57.98	71.84	53.77	63.85	31.77	34.82	50.02	61.60	50.87	62.15	68.46	78.62
metal_nut	82.95	87.73	91.58	94.73	83.82	85.42	88.38	90.73	91.17	93.57	85.52	90.20	79.55	84.46	92.57	96.16
pill	55.62	67.04	45.23	48.99	23.88	24.15	72.59	86.32	82.40	84.30	80.87	87.02	79.74	83.21	88.13	93.71
screw	4.88	6.63	25.08	35.77	12.32	13.11	22.35	23.78	38.14	40.36	23.23	29.91	30.65	40.21	33.01	46.06
tile	76.25	85.75	86.17	90.45	77.32	80.28	77.16	84.84	85.69	90.12	79.32	85.63	76.75	81.96	87.77	93.12
toothbrush	35.69	50.45	57.66	79.15	38.86	51.97	32.38	37.88	48.83	58.76	44.33	69.32	30.25	36.81	70.77	90.63
transistor	44.48	51.79	59.88	65.96	44.93	53.04	61.68	68.59	76.52	82.13	76.34	89.94	72.89	77.37	85.39	91.36
wood	35.51	46.00	49.82	62.09	36.41	51.10	47.29	61.35	51.84	63.70	52.06	72.75	52.48	60.68	74.26	80.58
zipper	51.61	63.09	66.88	75.75	61.99	70.07	66.09	77.54	60.61	71.11	57.86	67.64	59.43	71.57	69.28	79.89
Average	46.23	57.30	59.28	67.91	44.95	52.45	50.72	57.24	57.92	63.48	56.44	67.09	53.02	60.17	70.57	80.39

TABLE III
EVALUATION OF PIXEL-LEVEL SEGMENTATION ACCURACY ON EXTENDED BTAD DATA USING SEGFORMER AND BISENET V2.

Backbone	Category	CutPaste		DRAEM		GLASS		DFMGAN		RealNet		AnomalyDiffusion		DDGAN		SARD	
		mIoU ↑	Acc ↑	mIoU ↑	Acc ↑	mIoU ↑	Acc ↑	mIoU ↑	Acc ↑	mIoU ↑	Acc ↑	mIoU ↑	Acc ↑	mIoU ↑	Acc ↑	mIoU ↑	Acc ↑
Segformer	01	66.94	78.20	67.86	80.14	68.02	79.57	67.02	78.03	67.17	80.20	66.55	76.31	65.35	74.37	75.08	84.69
	02	65.04	83.64	69.52	82.96	69.99	83.58	68.75	84.92	70.64	83.90	68.06	84.74	60.09	71.70	69.86	81.21
	03	50.96	60.41	50.39	54.30	51.77	53.53	38.95	41.55	48.76	57.50	54.85	80.20	69.26	76.03	78.22	85.47
BiseNet V2	01	57.15	69.88	49.16	63.48	44.09	50.57	49.49	59.20	45.45	57.65	46.66	55.18	48.42	58.20	57.17	68.55
	02	59.45	82.05	66.46	80.29	66.37	79.46	66.02	79.21	66.11	81.67	65.57	84.00	57.53	71.11	67.34	81.01
	03	31.84	40.62	36.15	39.04	30.80	37.15	20.12	21.48	29.55	33.11	42.27	74.41	68.09	80.39	76.35	91.08

We further validate the generalization of SARD on the BTAD dataset, as shown in Table III. SARD again delivers superior performance across all categories under both segmentation backbones. Notably, on class 03, which contains fine-grained and spatially sparse defects, SARD achieves an mIoU of 78.22 with SegFormer and 76.35 with BiseNet V2, surpassing all baselines by a large margin. These improvements demonstrate the effectiveness of segmentation-aware Anomaly Synthesis in realistic industrial conditions.

Anomaly Synthesis Quality. Fig. 2 compares visual results of different anomaly synthesis methods on representative MVTEC categories. Traditional methods like CutPaste and DRAEM often generate artifacts with sharp transitions or unnatural boundaries. GAN-based approaches such as RealNet and DFMGAN improve texture realism but may introduce semantic misalignment or background inconsistencies.

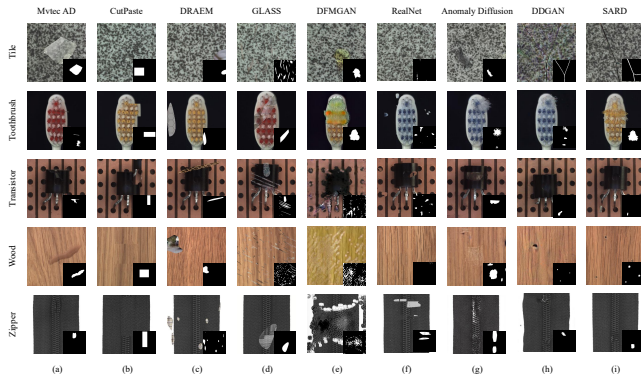


Fig. 2. Visual comparison of anomaly synthesis results on MVTEC-AD. Each column represents a synthesis method (CutPaste, DRAEM, Glass, RealNet, DFMGAN, AnomalyDiffusion, DDGAN, and SARD). Results illustrate boundary precision and texture quality.

In contrast, SARD produces anomaly textures that are mask-

aligned, structurally coherent, and well integrated with the surrounding context. The synthesized anomalies exhibit high visual fidelity and accurate boundary adherence, especially in categories like *metal_nut*, *tile*, and *transistor*, demonstrating the advantages of RCD and DMG in achieving segmentation-oriented synthesis.

C. Ablation Studies

Effect of Region-Constrained Diffusion (RCD). We first assess the impact of RCD by comparing against a baseline variant where the entire reverse denoising process follows the standard DDPM formulation without background preservation. That is, the full image is updated at each step, and no region-wise fusion is applied. As shown in Table IV, enabling RCD consistently improves mIoU and pixel-wise accuracy across most categories. For example, in *bottle*, mIoU increases from **66.75** to **77.19**, and in *capsule*, from **40.42** to **54.25**. These improvements demonstrate that restricting the denoising process to anomaly regions helps preserve background integrity and yields sharper, more localized defects.

Effect of Discriminative Mask Guidance (DMG). We then examine the effect of DMG by removing the mask-guided foreground branch from the discriminator, leaving only global image-level supervision. Without region-specific feedback, the generator tends to produce less coherent structures. Adding DMG improves performance in categories with complex textures or irregular boundaries. For instance, in *grid*, mIoU rises from **47.56** to **51.20**, and in *leather*, from **58.51** to **67.45**. This highlights the effectiveness of localized adversarial learning in guiding anomaly synthesis towards finer boundary alignment and textural fidelity.

TABLE IV
ABLATION STUDY OF RCD AND DMG COMPONENTS IN SARD USING
SEGFORMER ON MVTEC-AD.

Category	DDGAN (Baseline)		w/ RCD		w/ DMG		SARD	
	mIoU ↑	Acc ↑	mIoU ↑	Acc ↑	mIoU ↑	Acc ↑	mIoU ↑	Acc ↑
bottle	66.75	70.70	77.19	80.22	80.61	84.29	83.52	87.71
cable	55.83	61.67	64.12	63.41	62.60	68.22	70.76	76.60
capsule	40.42	48.74	54.25	53.82	51.59	61.92	61.25	71.04
carpet	67.98	79.25	71.04	74.19	73.31	83.88	76.39	84.77
grid	47.56	47.99	51.80	61.45	51.20	57.88	53.15	67.56
hazel_nut	63.77	68.33	74.72	81.04	69.05	73.12	79.30	82.50
leather	58.51	70.41	64.48	69.26	67.45	75.96	72.38	80.16
metal_nut	87.27	90.22	88.84	88.64	91.18	93.08	94.27	96.55
pill	84.69	90.90	86.71	86.43	85.69	90.13	89.02	92.99
screw	37.32	48.07	46.81	55.29	44.44	56.02	53.36	64.27
tile	82.42	89.25	84.39	86.70	89.16	93.75	90.32	94.77
toothbrush	35.36	40.98	64.88	74.36	67.45	83.83	72.77	91.58
transistor	77.96	81.75	81.16	87.55	84.46	84.68	89.60	94.24
wood	56.90	62.33	69.79	80.45	76.94	87.86	78.85	88.34
zipper	67.09	78.29	68.38	74.26	68.47	75.63	72.46	81.65

Conclusion. RCD and DMG each provide distinct but complementary advantages: RCD ensures structural consistency by freezing the background during generation, while DMG enhances foreground realism via spatially aware discrimination. Their combination—the complete SARD framework—yields the strongest results across all categories, demonstrating the necessity of jointly modeling background preservation and region-specific supervision in diffusion-based anomaly synthesis.

V. CONCLUSION

We presented SARD, a segmentation-aware anomaly synthesis framework designed for industrial inspection tasks. By incorporating Region-Constrained Diffusion (RCD) and Discriminative Mask Guidance (DMG), our method effectively addresses common issues in generative anomaly synthesis, such as spatial misalignment and background distortion. RCD constrains the reverse diffusion process to foreground regions while preserving the background from forward diffusion, ensuring more precise localization. DMG enhances the discriminator with mask-aware supervision, guiding the generator to produce sharper and more semantically aligned anomalies.

Extensive experiments on MVTEC-AD and BTAD datasets, using multiple segmentation backbones, demonstrate that SARD consistently outperforms state-of-the-art baselines. Ablation studies further confirm that both RCD and DMG provide distinct yet complementary benefits. These findings highlight the importance of jointly enforcing structural constraints and region-specific adversarial learning in diffusion-based anomaly synthesis.

REFERENCES

- [1] C.-L. Li, K. Sohn, J. Yoon, and T. Pfister, “Cutpaste: Self-supervised learning for anomaly detection and localization,” in *Proceedings of the IEEE/CVF conference on computer vision and pattern recognition*, 2021, pp. 9664–9674.
- [2] V. Zavrtnik, M. Kristan, and D. Skočaj, “Draem-a discriminatively trained reconstruction embedding for surface anomaly detection,” in *Proceedings of the IEEE/CVF international conference on computer vision*, 2021, pp. 8330–8339.
- [3] S. Niu, B. Li, X. Wang, and H. Lin, “Defect image sample generation with gan for improving defect recognition,” *IEEE Transactions on Automation Science and Engineering*, vol. 17, no. 3, pp. 1611–1622, 2020.
- [4] Y. Duan, Y. Hong, L. Niu, and L. Zhang, “Few-shot defect image generation via defect-aware feature manipulation,” in *Proceedings of the AAAI Conference on Artificial Intelligence*, vol. 37, no. 1, 2023, pp. 571–578.
- [5] J. Ho, A. Jain, and P. Abbeel, “Denoising diffusion probabilistic models,” *Advances in neural information processing systems*, vol. 33, pp. 6840–6851, 2020.
- [6] Y. Song, J. Sohl-Dickstein, D. P. Kingma, A. Kumar, S. Ermon, and B. Poole, “Score-based generative modeling through stochastic differential equations,” in *International Conference on Learning Representations*, 2021. [Online]. Available: <https://openreview.net/forum?id=PXTIG12RRHS>
- [7] R. Rombach, A. Blattmann, D. Lorenz, P. Esser, and B. Ommer, “High-resolution image synthesis with latent diffusion models,” in *Proceedings of the IEEE/CVF conference on computer vision and pattern recognition*, 2022, pp. 10 684–10 695.
- [8] P. Bergmann, M. Fauser, D. Sattlegger, and C. Steger, “Mvtec ad—a comprehensive real-world dataset for unsupervised anomaly detection,” in *Proceedings of the IEEE/CVF conference on computer vision and pattern recognition*, 2019, pp. 9592–9600.
- [9] P. Bergmann, K. Batzner, M. Fauser, D. Sattlegger, and C. Steger, “Btad: A balanced texture anomaly dataset for industrial visual inspection,” *arXiv preprint arXiv:2001.00495*, 2020.
- [10] E. Xie, W. Wang, Z. Yu, A. Anandkumar, J. M. Alvarez, and P. Luo, “Segformer: Simple and efficient design for semantic segmentation with transformers,” *Advances in neural information processing systems*, vol. 34, pp. 12 077–12 090, 2021.
- [11] C. Yu, C. Gao, J. Wang, G. Yu, C. Shen, and N. Sang, “Bisenet v2: Bilateral network with guided aggregation for real-time semantic segmentation,” *International journal of computer vision*, vol. 129, pp. 3051–3068, 2021.
- [12] Q. Chen, H. Luo, C. Lv, and Z. Zhang, “A unified anomaly synthesis strategy with gradient ascent for industrial anomaly detection and localization,” in *European Conference on Computer Vision*. Springer, 2025, pp. 37–54.
- [13] X. Zhang, M. Xu, and X. Zhou, “Realnet: A feature selection network with realistic synthetic anomaly for anomaly detection,” in *Proceedings of the IEEE/CVF Conference on Computer Vision and Pattern Recognition*, 2024, pp. 16 699–16 708.
- [14] Y. Li, J. Zhang, G.-J. Qi, and Z. Li, “Anomalydiffusion: A generative prior for unsupervised anomaly detection,” in *ICCV*, 2023.
- [15] M. Xiao, H. Hu, X. Wang, Y. Li, C. Wang, and Y. Wang, “Tackling the generative learning trilemma with denoising diffusion gans,” in *NeurIPS*, 2022.
- [16] G. Zhang, K. Cui, T.-Y. Hung, and S. Lu, “Defect-gan: High-fidelity defect synthesis for automated defect inspection,” in *Proceedings of the IEEE/CVF Winter Conference on Applications of Computer Vision*, 2021, pp. 2524–2534.
- [17] Z. Du, L. Gao, and X. Li, “A new contrastive gan with data augmentation for surface defect recognition under limited data,” *IEEE Transactions on Instrumentation and Measurement*, vol. 72, pp. 1–13, 2022.
- [18] S. Mou, R. Vemulapalli, S. Li, Y. Liu, C. Thomas, M. Cao, H. Bai, O. Tuzel, P. Huang, J. Shan *et al.*, “Synth4seg—learning defect data synthesis for defect segmentation using bi-level optimization,” *arXiv preprint arXiv:2410.18490*, 2024.
- [19] H. Xu, Y. Wang, J. Wei, S. Jian, Y. Li, and N. Liu, “Fascinating supervisory signals and where to find them: Deep anomaly detection with scale learning,” in *International Conference on Machine Learning*. PMLR, 2023, pp. 38 655–38 673.
- [20] M. Yang, J. Liu, Z. Yang, and Z. Wu, “Slsg: Industrial image anomaly detection with improved feature embeddings and one-class classification,” *Pattern Recognition*, vol. 156, p. 110862, 2024.
- [21] X. Liu, J. Wang, B. Leng, and S. Zhang, “Dual-modeling decouple distillation for unsupervised anomaly detection,” in *Proceedings of the 32nd ACM International Conference on Multimedia*, 2024, pp. 5035–5044.
- [22] T. Hu, J. Zhang, R. Yi, Y. Du, X. Chen, L. Liu, Y. Wang, and C. Wang, “Anomalydiffusion: Few-shot anomaly image generation with diffusion model,” in *Proceedings of the AAAI Conference on Artificial Intelligence*, vol. 38, no. 8, 2024, pp. 8526–8534.